



General dual-band coordinate transformation media with full-tensor anisotropic dispersion controlsYuma Takano * and Atsushi Sanada *Graduate School of Engineering Science, Osaka University, Osaka 560-8531, Japan*

(Received 20 June 2021; revised 1 September 2021; accepted 27 September 2021; published 7 October 2021)

We propose general dual-band coordinate transformation media realizing two arbitrary coordinate transformations at two target frequencies and their universal implementation method by LC-based circuit metamaterials with full-tensor anisotropic dispersion controls. The circuit topologies to fully manipulate the material parameters to be realized are discussed. The general quantitative relations of the equivalent material parameters in two arbitrary coordinate transformations are classified into six cases, and the five fundamental branch unit constituents to cover all the six cases are presented. As an example, a dual-band illusion device with peculiar dispersions mimicking a bump and a pothole at each frequency is designed based on the presented implementation method. The illusion operations of the designed medium for 0 and 45° incidences are numerically demonstrated by circuit simulations, and the validities of the proposed concept and the implementation method are confirmed.

DOI: [10.1103/PhysRevB.104.165115](https://doi.org/10.1103/PhysRevB.104.165115)**I. INTRODUCTION**

Based on the concept of transformation electromagnetics [1], various coordinate transformation media such as invisibility cloaks hiding objects [2–12] and illusion devices making an object appear exactly like another object [13–16] have been proposed. Many coordinate transformation media presented so far can effectively realize one coordinate transformation at a single target frequency [see Fig. 1(a)]. In contrast, there are a limited number of studies seeking dual-band (or multi-band) coordinate transformation media. To realize dual-band operations, dispersions of full-tensor anisotropic material parameters need to be fully manipulated.

LC-based circuit metamaterials [17–23], which are metamaterials composed of LC-lumped element circuit networks with full controls of effective permittivity and permeability, are potentially capable of dual-band operations. References [21] and [22] have proposed dual-band cylindrical cloaks of invisibility based on LC-based circuit metamaterials realizing one identical coordinate transformation at two target frequencies [see Fig. 1(b)] by controlling the dispersion of a single diagonal component. In [23], LC-based circuit metamaterials realizing two different coordinate transformations at two target frequencies have been proposed. The proposed circuit metamaterials can only realize two specific coordinate transformations for which the dispersions of the equivalent material parameters are the Drude-like dispersions with two lumped elements in each circuit branch; i.e., according to Foster's reactance theorem [24], the reactance at the lower frequency must always be smaller than that at the higher frequency. A universal implementation method is necessary to realize general dual-band coordinate transformation media for two arbitrary coordinate transformations with peculiar dispersions which do not follow Drude's model such that the

reactance at the lower frequency is larger than that at the higher frequency.

The above-mentioned peculiar dispersions can be artificially engineered by LC-based metamaterials with appropriate circuit topologies based on the physical perspective that material dispersions are directly associated with lumped element circuitries. The governing equations of circuit networks are identical to the discretized Maxwell equations and designing circuit topologies is controlling material dispersions in a physical sense. The solutions of the circuit equations become identical to those of Maxwell equations in the dispersive media if the discretization size is small enough compared to the wavelength.

In this paper, we propose general dual-band coordinate transformation media realizing two arbitrary coordinate transformations at two target frequencies based on LC-based circuit metamaterials [see Fig. 1(c)]. The dispersions of the full-tensor anisotropic material parameters including the off-diagonal components are fully manipulated, regardless of the quantitative relations of the equivalent material parameters for the two coordinate transformations. We also discuss the universal implementation method to determine circuit topologies and parameters. As an example, a dual-band illusion device with peculiar dispersions is designed based on the implementation method, and the dual-band illusion operations are numerically discussed to confirm the validities of the proposed concept and the implementation method.

II. GENERAL DUAL-BAND COORDINATE TRANSFORMATION MEDIA

Here, let us discuss tensor parameters and circuit topology for dispersion controls needed to realize general dual-band coordinate transformation media. Henceforth throughout the paper, we deal with passive lossless systems considering realistic loss systems in which the attenuation constants are small.

*y-takano@ec.ee.es.osaka-u.ac.jp

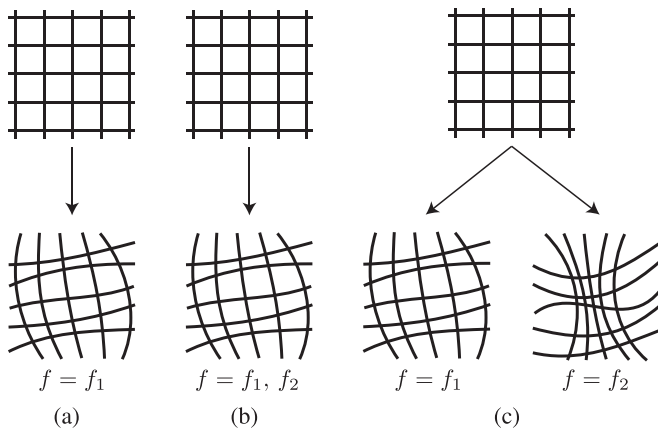


FIG. 1. Single- and dual-band coordinate transformations. (a) Conventional single coordinate transformation at a single frequency. (b) Conventional single coordinate transformation at dual frequencies. (c) Proposed concept of two arbitrary coordinate transformations at dual frequencies.

A. Tensor parameters and circuit topology

According to the transformation electromagnetics [1], equivalent material parameters of a coordinate transformation from a coordinate system (x', y') to another coordinate system (x, y) are given as

$$\varepsilon^{ij} = \mu^{ij} = \frac{\delta^{i'j'} \Lambda_{i'}^i \Lambda_{j'}^j}{\det(\Lambda_{i'}^i)}, \quad (1)$$

where $\Lambda_{i'}^i \equiv \partial x^i / \partial x^{i'}$ is the Jacobi matrix of the coordinate transformation. For two-dimensional TM waves propagating in the xy plane, the material parameters to be controlled are

$$\bar{\varepsilon} = \begin{pmatrix} \varepsilon_{xx} & \varepsilon_{xy} \\ \varepsilon_{yx} & \varepsilon_{yy} \end{pmatrix}, \quad \mu_{zz}, \quad (2)$$

where $\varepsilon_{xy} = \varepsilon_{yx}$.

The circuit topologies to realize coordinate transformation media based on LC-based circuits are shown in Fig. 2, where Z_i ($i = x, y, m$) represent the impedances in the corresponding branches, and Y represents the admittance in the shunt branch. Δd is the unit cell size. Hereinafter, we refer to the

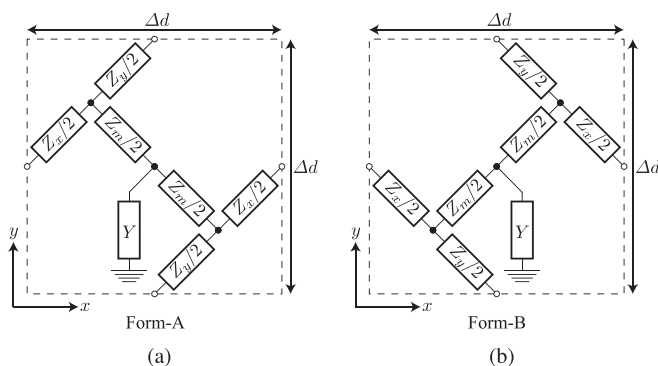


FIG. 2. Circuit topologies of general dual-band coordinate transformation media. (a) Form A. (b) Form B. Forms A and B are isomer circuits of each other with different signs in the off-diagonal components.

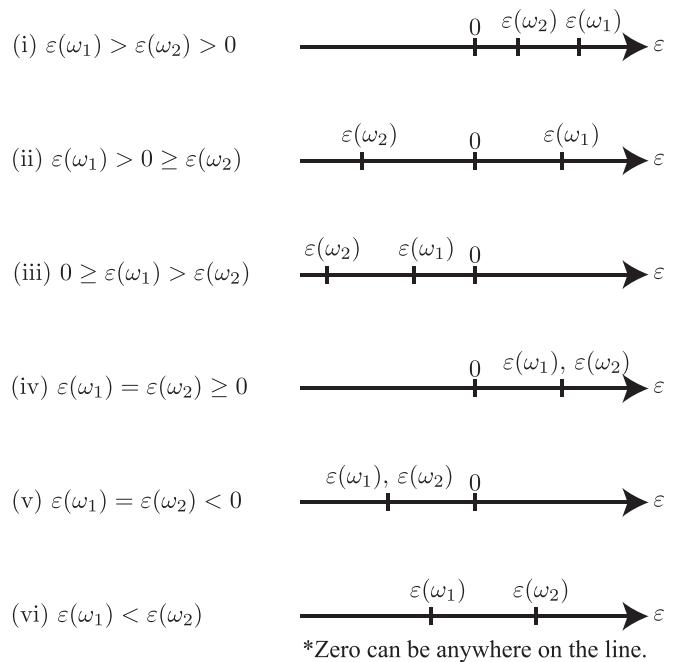


FIG. 3. Six cases of the general quantitative relation between the permittivities at two frequencies.

unit circuits in Figs. 2(a) and 2(b) as Form A and Form B, respectively. The parameters Z_i and Y are to be given from the material parameters as [25,26]

$$Z_x = j\omega(\varepsilon_{yy} \mp \varepsilon_{xy})\Delta d, \quad (3a)$$

$$Z_m = \pm j\omega\varepsilon_{xy}\Delta d, \quad (3b)$$

$$Z_y = j\omega(\varepsilon_{xx} \mp \varepsilon_{xy})\Delta d, \quad (3c)$$

$$Y = j\omega\mu_{zz}\Delta d, \quad (3d)$$

where the double signs correspond to the cases for Forms A and B, respectively. It should be noted that the relations between the branch unit components (Z_i, Y) and the material parameters (ε, μ) are exchanged from those in the conventional telegrapher's equations; i.e., (Z_i, Y) correspond to (μ, ε), owing to the TE and TM duality. Based on (3), we can independently manipulate the permeability and the permittivity tensor including the off-diagonal component. It is noted that Forms A and B are isomer circuits of each other with different signs in the off-diagonal components, which can be used as a design degree of freedom.

B. Dispersive branch unit constituents for general dual-band coordinate transformation media

First, we discuss the relation between the permittivity and the impedance in (3a)–(3c). Let us consider two arbitrary different coordinate transformations at two arbitrary different frequencies, f_1 ($=\omega_1/2\pi$) and f_2 ($=\omega_2/2\pi > f_1$). The quantitative relation between the permittivities at these frequencies, $\varepsilon(\omega_1)$ and $\varepsilon(\omega_2)$, can be classified into six cases (see Fig. 3):

- (i) $\varepsilon(\omega_1) > \varepsilon(\omega_2) > 0$,
- (ii) $\varepsilon(\omega_1) > 0 \geq \varepsilon(\omega_2)$,

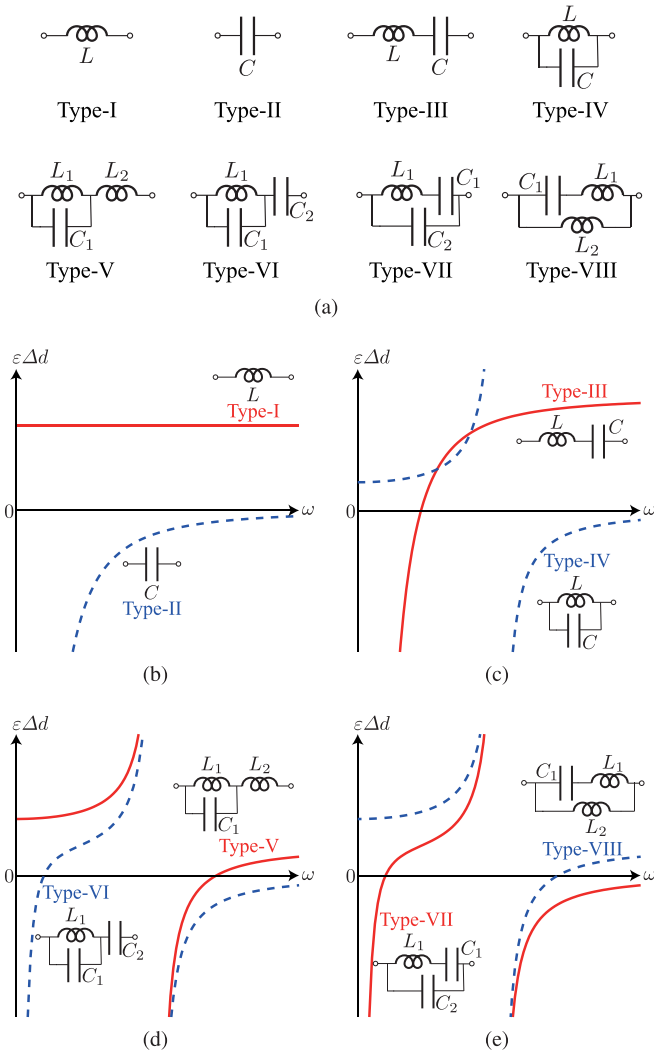


FIG. 4. Branch unit constituents and their dispersion behaviors. (a) All eight possible circuits consisting of fewer than three passive elements. The dispersion behaviors realized by the circuits are (b) Types I and II, (c) Types III and IV, (d) Types V and VI, and (e) Types VII and VIII.

- (iii) $0 \geq \varepsilon(\omega_1) > \varepsilon(\omega_2)$,
- (iv) $\varepsilon(\omega_1) = \varepsilon(\omega_2) \geq 0$,
- (v) $\varepsilon(\omega_1) = \varepsilon(\omega_2) < 0$,
- (vi) $\varepsilon(\omega_1) < \varepsilon(\omega_2)$,

where ε represents either of $\varepsilon_{yy} \mp \varepsilon_{xy}$, $\pm \varepsilon_{xy}$, or $\varepsilon_{xx} \mp \varepsilon_{xy}$, depending on the branch units, and the double signs correspond to the cases for Forms A and B. Figure 4(a) shows all eight circuits consisting of fewer than three passive elements to realize the quantitative relation, or the dispersion, of cases (i)–(vi): L (Type I), C (Type II), LC series (Type III), LC tank (Type IV), series circuit of LC tank and L (Type V), series circuit of LC tank and C (Type VI), parallel circuit of LC series and L (Type VII), and parallel circuit of LC series and C (Type VIII). Types I and II are one-element circuits, Types III and IV are two-element circuits, and Types V to VIII are three-element circuits. The dispersion behaviors of the permittivity realized by Types I to VIII are shown in Figs. 4(b)–4(e).

TABLE I. Correspondence between the six cases of the quantitative relation and the number of circuit elements in the branch unit.

Cases	One element	Two elements	Three elements
(i)			✓
(ii)		✓	✓
(iii)			✓
(iv)	✓		
(v)			✓
(vi)		✓	✓

In the first case, (i), the quantitative relation of $\varepsilon(\omega_1) > \varepsilon(\omega_2) > 0$ can be realized by either of the three-element circuits of Type V or VIII. This is because, for a given positive $\varepsilon(\omega_1)$ larger than positive $\varepsilon(\omega_2)$, we need a single pole in the band and an inductive reactance at the infinite frequency, according to Foster's reactance theorem. Only Types V and VIII three-element circuits satisfy this condition. In the second case, (ii), the quantitative relation of $\varepsilon(\omega_1) > 0 \geq \varepsilon(\omega_2)$ can be realized by the two-element circuit of Type IV or by all the three-element circuits of Types V to VIII. In the third case, (iii), the quantitative relation of $0 \geq \varepsilon(\omega_1) > \varepsilon(\omega_2)$ can be realized by the three-element circuits of Type VI or VII. In the fourth case, (iv), the quantitative relation of $\varepsilon(\omega_1) = \varepsilon(\omega_2) \geq 0$ can be realized by the one-element circuit of Type I. In the fifth case, (v), the quantitative relation of $\varepsilon(\omega_1) = \varepsilon(\omega_2) < 0$ can be realized by the three-element circuits of Type VI or VII. And in the sixth case, (vi), the quantitative relation of $\varepsilon(\omega_1) < \varepsilon(\omega_2)$ can be realized by the two-element circuit of Type III or by all the three-element circuits of Types V to VIII. The correspondence between the six cases of the quantitative relation and the number of circuit elements in the branch unit is summarized in Table I. It should be noted that all the dispersions of cases (i)–(vi) can be realized only with the five circuits of Types I, III, IV, V, and VI. Incidentally, Type V is interchangeable with Type VIII, and Type VI is also interchangeable with Type VII, according to Figs. 4(d) and 4(e). It should also be noted that the third element degree of freedom is required in cases (i), (iii), and (v) to realize only two different material parameters under the constraint of Foster's reactance theorem.

A similar discussion can be applied to the relation between the permeability and the admittance in (3d). The relation between the permeabilities at the two frequencies, $\mu_{zz}(\omega_1)$ and $\mu_{zz}(\omega_2)$, can also be classified into the above six cases. Due to the duality of the admittance and the impedance, each of the admittance dispersions of the cases can be realized by the dual circuits of the five fundamental circuits: Types II, IV, III, VII, and VIII. Similarly, Type VII and Type VIII are interchangeable with Type VI and Type V, respectively.

III. EXAMPLE: DUAL-BAND ILLUSION DEVICE

A. Coordinate transformations and unit circuit topology

As an example to demonstrate a general dual-band coordinate transformation medium, we design a dual-band illusion device which exhibits scattering characteristics of a bump at a lower frequency, $f_1 = 28$ GHz, and that of a pothole at a

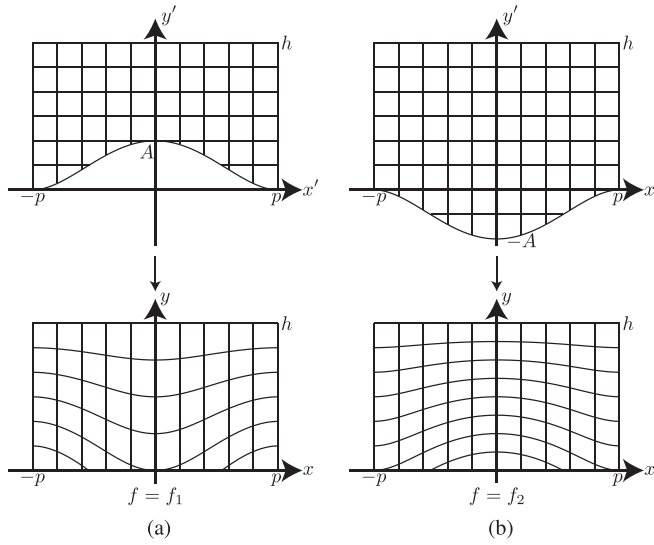


FIG. 5. Two coordinate transformations for the dual-band illusion device. (a) At $f = f_1$. (b) At $f = f_2$. In each panel, the upper original coordinate system is transformed into the lower coordinate system.

higher frequency, $f_2 = 32$ GHz. The coordinate transformations for the bump and the pothole are chosen to be

$$x = x' \quad \text{at} \quad f = f_1, f_2, \quad (4a)$$

$$y = \begin{cases} \frac{y'-A\left[1-\left(\frac{x'}{p}\right)^2\right]^2}{h-A\left[1-\left(\frac{x'}{p}\right)^2\right]^2} h & \text{at} \quad f = f_1, \\ \frac{y'+A\left[1-\left(\frac{x'}{p}\right)^2\right]^2}{h+A\left[1-\left(\frac{x'}{p}\right)^2\right]^2} h & \text{at} \quad f = f_2, \end{cases} \quad (4b)$$

where h corresponds to the device height, A corresponds to the bump height or the pothole depth, and p corresponds to the device half-width, as shown in Fig. 5. At f_1 , the space with a bump is transformed into a rectangular space of height h and width $2p$ as shown in Fig. 5(a). At f_2 , the space with a pothole is simultaneously transformed into the same rectangular space as shown in Fig. 5(b).

Equivalent material parameters calculated according to (1) with typical geometrical values of $h = 3\lambda_{\omega_0}$, $A = \lambda_{\omega_0}$, and $2p = 5\lambda_{\omega_0}$ are shown in Fig. 6, where λ_{ω_0} is the wavelength in free space at the angular frequency $\omega_0 = \sqrt{\omega_1\omega_2}$ in between ω_1 and ω_2 . These coordinate transformation yields y -axisymmetric nonextreme material parameters including off-diagonal components to be manipulated. According to Fig. 6, the quantitative relations of $\varepsilon(\omega_1)$ and $\varepsilon(\omega_2)$ are different depending on the positions and the components. We design the dual-band illusion device based on the discussion in Sec. II B.

Figure 7(a) shows the LC-circuit-type distributions of each branch unit determined based on the relations shown in Fig. 6 under the condition that the left half takes Form A and the right half takes Form B in accordance with the y axisymmetry of the system. Z_x is realized with the three-element circuit of Type V all over the region, and Z_m and Y are realized with the two-element circuits of Types III and IV all over the region, respectively, whereas Z_y has to be realized with

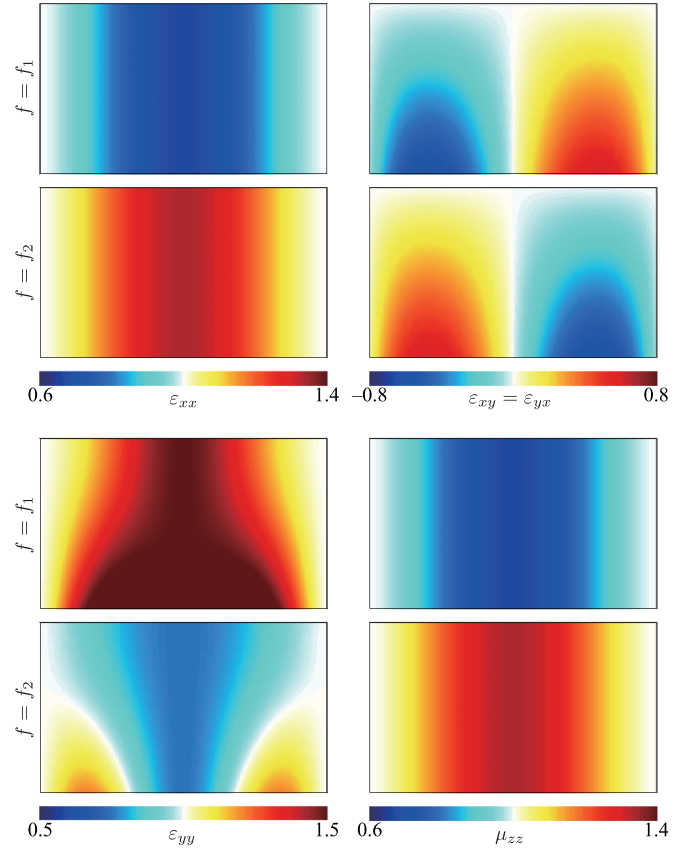


FIG. 6. Equivalent material parameters of the two coordinate transformations in Fig. 5 with $h = 3\lambda_{\omega_0}$, $A = \lambda_{\omega_0}$, and $2p = 5\lambda_{\omega_0}$.

two different types: the two-element circuit of Type III and the three-element circuit of Type V, as shown in Fig. 7(a). The resulting LC-based circuit metamaterial configuration is depicted in Fig. 7(b). The metamaterial is composed of four kinds of unit circuits.

B. Circuit parameters

As discussed in Sec. II B, the additional third element degree of freedom is introduced in Z_x and Z_y to realize the material parameter quantitative relation of $\varepsilon(\omega_1) > \varepsilon(\omega_2) > 0$. Here, we discuss how to determine the third degree of freedom as well as the other circuit parameters.

In the case of realizing two different values by the two-element circuit of Type III, the element values of L and C are uniquely determined from (3) with $Z(\omega) = j\omega L + 1/j\omega C$ as

$$L = \frac{\omega_2^2 \varepsilon(\omega_2) - \omega_1^2 \varepsilon(\omega_1)}{\omega_2^2 - \omega_1^2} \Delta d, \quad (5a)$$

$$C = \frac{1}{[\varepsilon(\omega_2) - \varepsilon(\omega_1)] \Delta d} \left(\frac{1}{\omega_1^2} - \frac{1}{\omega_2^2} \right). \quad (5b)$$

(Recall that ε represents either of $\varepsilon_{yy} \mp \varepsilon_{xy}$, $\pm \varepsilon_{xy}$, or $\varepsilon_{xx} \mp \varepsilon_{xy}$, depending on the branch units and the double signs correspond to the cases for Forms A and B.)

On the other hand, in the case of realizing two different values by the three-element circuit of Type V, there remains one degree of freedom. Here, we use the third degree of

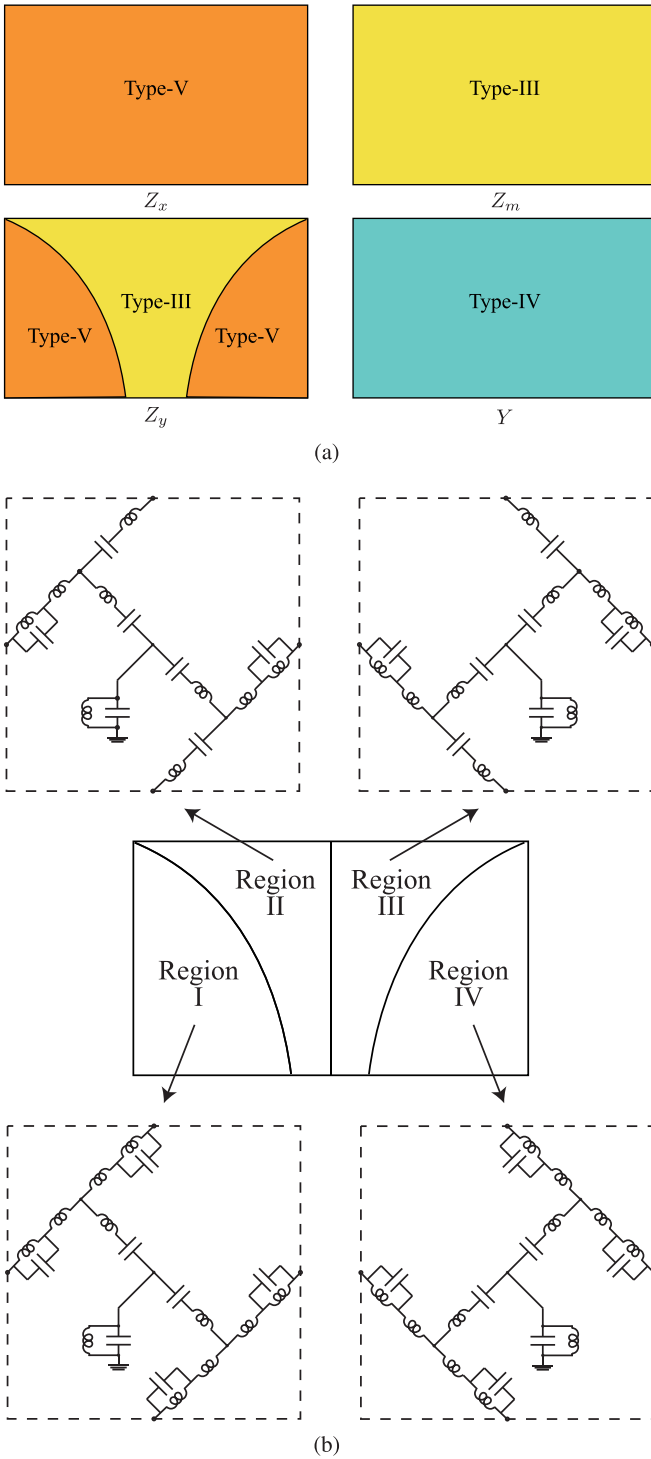


FIG. 7. LC-circuit-type distributions and metamaterial configuration in the illusion device. (a) LC-circuit-type distributions of each branch unit. (b) Resulting LC-based circuit metamaterial configuration.

freedom so that the resonant frequency of the LC-tank circuit becomes $1/\sqrt{L_1 C_1} = \sqrt{\omega_1 \omega_2} (= \omega_0)$ in the range between ω_1 and ω_2 . This is advantageous in terms of the operation bandwidth since ω_0 is the farthest frequency from both ω_1 and ω_2 , and also the dispersion is less frequency dependent as the frequency becomes farther from the resonant frequency.

In addition, even in a realistic lossy system, this off-resonant operation is also advantageous in terms of losses for a similar reason. The element values of Type V are determined by giving this LC-tank resonant frequency to (3) with $Z(\omega) = j\omega L_2 + 1/(1/j\omega L_1 + j\omega C)$ as

$$L_1 = \frac{\omega_2 - \omega_1}{\omega_2 + \omega_1} [\varepsilon(\omega_1) - \varepsilon(\omega_2)] \Delta d, \quad (6a)$$

$$L_2 = \frac{\omega_2 \varepsilon(\omega_2) + \omega_1 \varepsilon(\omega_1)}{\omega_2 + \omega_1} \Delta d, \quad (6b)$$

$$C_1 = \frac{1}{[\varepsilon(\omega_1) - \varepsilon(\omega_2)] \Delta d} \frac{\omega_2 + \omega_1}{\omega_1 \omega_2 (\omega_2 - \omega_1)}. \quad (6c)$$

As for the admittance Y of Type IV, due to the duality of the impedance and the admittance and the duality of Types III and IV, the circuit parameters are simply given by taking the dual of (5) as

$$C = \frac{\omega_2^2 \mu_{zz}(\omega_2) - \omega_1^2 \mu_{zz}(\omega_1)}{\omega_2^2 - \omega_1^2} \Delta d, \quad (7a)$$

$$L = \frac{1}{[\mu_{zz}(\omega_2) - \mu_{zz}(\omega_1)] \Delta d} \left(\frac{1}{\omega_1^2} - \frac{1}{\omega_2^2} \right). \quad (7b)$$

With these equations of (5)–(7), all the circuit parameters in Regions I–IV in Fig. 7(b) are determined.

Incidentally, in different designs with different coordinate transformations, different types of circuits in Fig. 4(a) might be required. Even in such cases, the circuit parameters are also determined in a similar manner.

C. Numerical simulations

In order to confirm the validity of the proposed concept of general dual-band coordinate transformation media and their universal implementation method, we carry out circuit simulations for the dual-band illusion device designed above using a SPICE simulator. The circuit parameters are calculated based on (5)–(7) with the unit cell size $\Delta d = \lambda_{\omega_0}/20$. The detailed circuit parameter calculations and the calculated circuit parameters are shown in the Supplemental Material [27].

Figure 8 shows the schematic and the boundary conditions of the circuit simulations. We prepare a node list of $n_x \times n_y = 150 \times 130$ unit cells for the entire computational area of $7.5\lambda_{\omega_0} \times 6.5\lambda_{\omega_0}$. The unit circuits in Fig. 7(b) are arranged in Regions I–IV. The unit circuits in the other regions are set to be those for free space, i.e., $Z_x = Z_y = j\omega L = j\omega \varepsilon_0 \Delta d$, $Z_m = 0$, and $Y = j\omega C = j\omega \mu_0 \Delta d$, where the characteristic impedance is $1/\eta_0 \equiv \sqrt{\varepsilon_0/\mu_0} \simeq 2.7 \times 10^{-3} \Omega$. Note that (Z_i, Y) and (ε, μ) are exchanged in the TM simulations. The nodes on the bottom row are open-circuited to mimic a perfect electric conductor floor. Four hundred ten voltage sources are connected at the nodes on the other periphery with the internal impedance of $2.7 \times 10^{-3} \Omega$ as shown by the blue lines in Fig. 8. The amplitude and phase of the voltage sources are set so as to form a Gaussian beam of beam waist $2\lambda_{\omega_0}$ with the incident angles of 0 and 45°. For comparison, two kinds of additional simulations are carried out for the original area with a bump and for that with a pothole shown in Fig. 5. In these simulations, all the unit cells are composed of the identical free-space circuits and all the

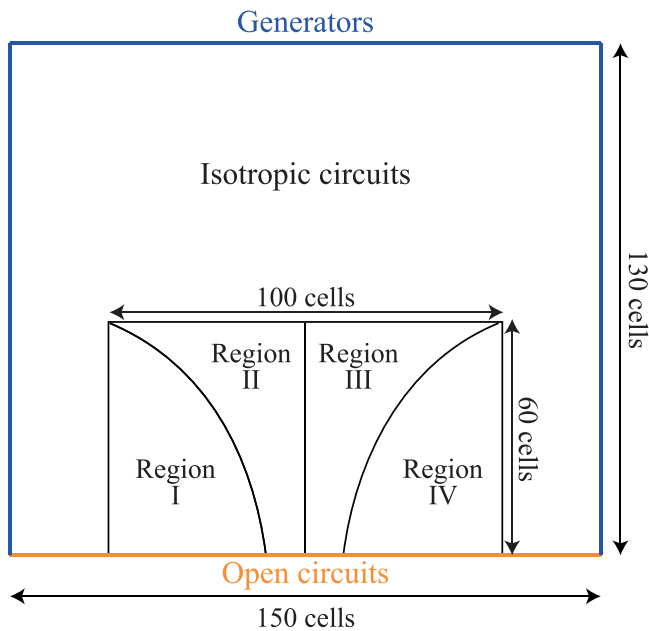


FIG. 8. Schematic and boundary conditions of the circuit simulations.

boundary conditions are set to be the same as the illusion simulations. In the pothole simulations, the computational area is extended by 20 cells at the bottom to accommodate the pothole.

Figure 9(a) shows the simulated voltage amplitude distributions at the center nodes in the unit cells for the vertical incidence at both f_1 and f_2 . The illusion device is placed in the dashed rectangular area. It is shown in the figure that the illusion device successfully mimics both the bump at 28 GHz and the pothole at 32 GHz. Figure 9(b) also shows the scattering characteristics for the 45° incidence at those frequencies. It is also shown in the figure that the illusion device successfully mimics the original area at both 28 and 32 GHz, which is the consequence of the angle-independent nature of transformation electromagnetics. With these results, the dual-band illusion operation is qualitatively confirmed.

In order to quantitatively confirm the illusion operation, bistatic radar cross sections (BRCSs) at these frequencies are calculated from the simulated amplitude distributions. The calculated BRCSs are shown for the incident angles of 0° in Fig. 10(a) and 45° in Fig. 10(b). In the figures, the solid red lines represent the BRCSs for the dual-band illusion device, the dashed blue lines represent those for the bump, and the dashed green lines represent those for the pothole. According to Fig. 10(a), the BRCS for the dual-band illusion device agrees well with that for the bump or the pothole. At 28 GHz, the BRCS for the illusion device has six major peaks at the same angles of $\pm 9^\circ$, $\pm 23^\circ$, and $\pm 51^\circ$ as those for the bump, whereas at 32 GHz, the BRCS for the illusion device has four major peaks at the same angles of $\pm 10^\circ$ and $\pm 35^\circ$ as those for the pothole. The maximum amplitude deviations at the peaks of the BRCSs are less than 7.9%, which is reasonable within the range of the discretization and the numerical errors. According to the results in Fig. 10(b) for the 45° incidence

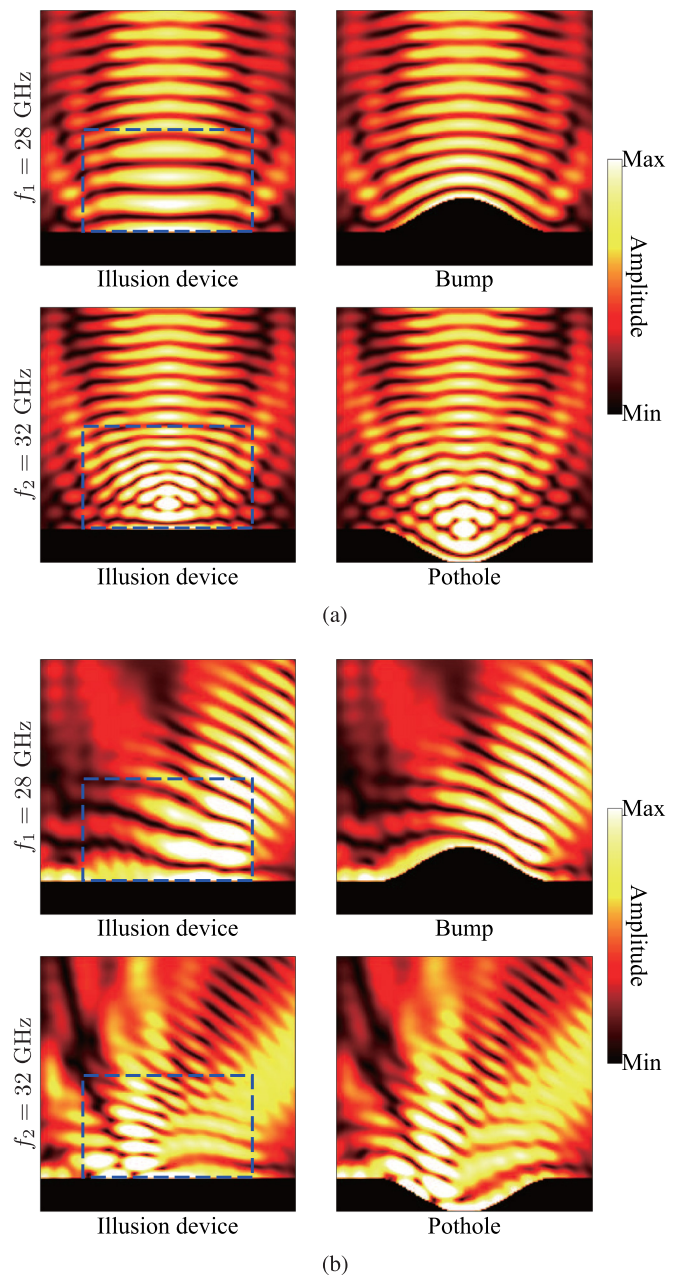


FIG. 9. Simulated scattering characteristics of the dual-band illusion device with those of the corresponding bump or pothole for (a) 0° incidence and (b) 45° incidence. The color bar is on a linear scale. The dual-band illusion device is arranged in the dashed rectangular region.

case, the BRCSs for the illusion device and the corresponding bump/pothole have the same major peak angles at both frequencies and agree well with each other. The maximum amplitude deviations at the peaks of the BRCSs are less than 5.4%. Based on these results, the dual-band illusion operation is quantitatively confirmed, which certifies the validities of the proposed concept and the implementation method.

IV. CONCLUSIONS

General dual-band coordinate transformation media realizing two arbitrary coordinate transformations at two

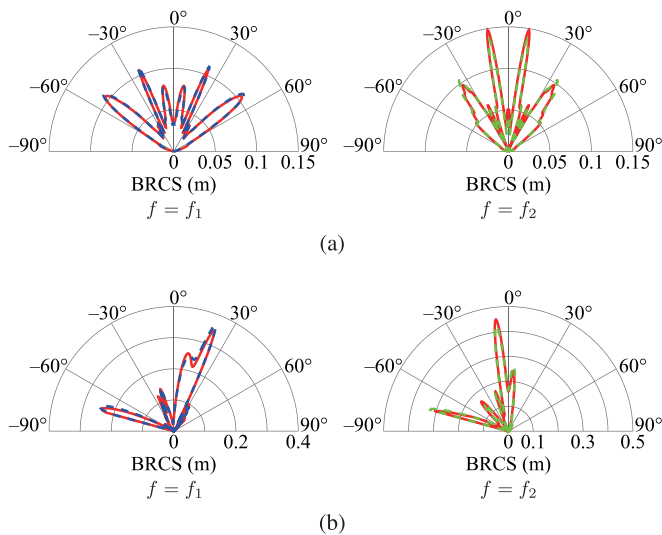


FIG. 10. BRCSs of the dual-band illusion device plotted together with those of the corresponding bump or pothole for (a) 0° incidence and (b) 45° incidence. The solid red line represents the BRCS of the illusion device, the dashed blue line represents that of the corresponding bump, and the dashed green line represents that of the corresponding pothole.

target frequencies have been proposed, and their universal implementation method by the LC-based circuit metamaterials with full-tensor anisotropic dispersion controls has been presented. The circuit topologies to fully manipulate the permittivity tensor and the permeability have been discussed. The quantitative relations of the equivalent material parameters in the two coordinate transformations have been classified into six cases, and the five fundamental branch unit dispersion control methods to cover all six cases have been presented. As an example, a dual-band illusion device has been designed based on the implementation method, and its illusion operation has been numerically demonstrated by circuit simulations. The simulated field distributions and the corresponding BRCSs for 0° and 45° incidences have revealed the proper operation of the dual-band illusion device both qualitatively and quantitatively. The validities of the proposed concept and the implementation method have been confirmed.

ACKNOWLEDGMENT

This work was supported by JSPS KAKENHI Grant No. 19J20104.

- [1] J. B. Pendry, D. Schurig, and D. R. Smith, *Science* **312**, 1780 (2006).
- [2] D. Schurig, J. J. Mock, B. J. Justice, S. A. Cummer, J. B. Pendry, A. F. Starr, and D. R. Smith, *Science* **314**, 977 (2006).
- [3] W. Cai, U. K. Chettiar, A. V. Kildishev, V. M. Shalaev, and G. W. Milton, *Appl. Phys. Lett.* **91**, 111105 (2007).
- [4] W. Cai, U. K. Chettiar, A. V. Kildishev, and V. M. Shalaev, *Nat. Photonics* **1**, 224 (2007).
- [5] J. Li and J. B. Pendry, *Phys. Rev. Lett.* **101**, 203901 (2008).
- [6] R. Liu, C. Ji, J. J. Mock, J. Y. Chin, T. J. Cui, and D. R. Smith, *Science* **323**, 366 (2009).
- [7] J. Valentine, J. Li, T. Zentgraf, G. Bartal, and X. Zhang, *Nat. Mater.* **8**, 568 (2009).
- [8] T. Ergin, N. Stenger, P. Brenner, J. B. Pendry, and M. Wegener, *Science* **328**, 337 (2010).
- [9] H. F. Ma and T. J. Cui, *Nat. Commun.* **1**, 21 (2010).
- [10] X. Chen, Y. Luo, J. Zhang, K. Jiang, J. B. Pendry, and S. Zhang, *Nat. Commun.* **2**, 176 (2011).
- [11] N. Landy and D. R. Smith, *Nat. Mater.* **12**, 25 (2013).
- [12] Y. Takano and A. Sanada, *EPJ Appl. Metamat.* **7**, 4 (2020).
- [13] Y. Lai, J. Ng, H. Y. Chen, D. Z. Han, J. J. Xiao, Z.-Q. Zhang, and C. T. Chan, *Phys. Rev. Lett.* **102**, 253902 (2009).
- [14] W. X. Jiang, H. F. Ma, Q. Cheng, and T. J. Cui, *Appl. Phys. Lett.* **96**, 121910 (2010).
- [15] Y. Xu, S. Du, L. Gao, and H. Chen, *New J. Phys.* **13**, 023010 (2011).
- [16] W. X. Jiang and T. J. Cui, *Phys. Rev. E* **83**, 026601 (2011).
- [17] X. Liu, C. Li, K. Yao, X. Meng, W. Feng, B. Wu, and F. Li, *Appl. Phys. Lett.* **95**, 191107 (2009).
- [18] C. Li, X. Meng, X. Liu, F. Li, G. Fang, H. Chen, and C. T. Chan, *Phys. Rev. Lett.* **105**, 233906 (2010).
- [19] C. Li, X. Liu, G. Liu, F. Li, and G. Fang, *Appl. Phys. Lett.* **99**, 084104 (2011).
- [20] M. Liu, Z. Lei Mei, X. Ma, and T. J. Cui, *Appl. Phys. Lett.* **101**, 051905 (2012).
- [21] H. Zhang, H. Xin, and R. W. Ziolkowski, in *2009 IEEE Antennas and Propagation Society International Symposium (IEEE, Piscataway, NJ, 2009)*, pp. 1–4.
- [22] J. Shao, H. Zhang, Y. Lin, and X. Hao, *Prog. Electromagn. Res.* **119**, 225 (2011).
- [23] Y. Takano and A. Sanada, in *2020 IEEE International Symposium on Radio-Frequency Integration Technology (RFIT)* (IEEE, Piscataway, NJ, 2020), pp. 55–57.
- [24] R. M. Foster, *Bell Syst. Tech. J.* **3**, 259 (1924).
- [25] T. Nagayama and A. Sanada, *IEEE Trans. Microwave Theory Techn.* **63**, 3851 (2015).
- [26] T. Nagayama and A. Sanada, *EPJ Appl. Metamat.* **6**, 23 (2019).
- [27] See Supplemental Material at <http://link.aps.org/supplemental/10.1103/PhysRevB.104.165115> for the detailed calculations of the circuit parameters.